International Journal of
INTELLIGENT SYSTEMS AND APPLICATIONS IN ENGINEERING

ISSN:2147-6799 www.ijisae.org Original Research Paper

A Proposed CNN-based Hybrid Deep Learning Model for the Segmentation of Multi-organ Functional Tissue Units

Anubhav De[1], Vineet Joon*[2], Nilamadhab Mishra*[3]

Submitted: 28/05/2023 **Revised**: 15/07/2023 **Accepted**: 30/07/2023

Abstract: In order to provide effective techniques for identifying and segmenting organs in high-resolution histology pictures, this research paper introduces a deep learning approach to the HubMAP-Organ Segmentation Competition. The proposed solution combines a Convolutional Neural Network with a U-Net architecture to achieve state-of-the-art performance on the competition's validation dataset. Extensive experiments have also been performed to analyze the effect of different hyperparameters and preprocessing techniques on the model performance and also the usage of different pre-trained models such as AlexNet, ZFNet, and EfficientNet. Our proposed CNN-based hybrid model claims to achieve a mean Dice Coefficient/Accuracy of 0.84178 on each image in the test set highlighting the effectiveness of our approach and providing insights into organ segmentation in high-resolution histology images, which has important applications in medical diagnosis and research.

Keywords: *Multi-Organ Segmentation, Functional Tissue Units, Deep Learning, U-Net Architecture, Convolutional Neural Networks, Image Masking*

1. Introduction

Organ Segmentation is a very important task in medical image analysis because segmentation done accurately can improve the diagnosis and treatment of diseases and also help in understanding the body's complex physiology. Deep Learning techniques in recent years have shown promising results in the field of medicine. The HuBMAP consortium The HubMap Organ Segmentation Challenge, hosted by Kaggle, is a platform for researchers and data scientists to develop new techniques for segmenting human tissue samples from medical images. The challenge presents a unique opportunity to address one of the most significant problems in medical imaging - the accurate segmentation of organs and tissues. Medical imaging is a critical tool in healthcare, allowing clinicians to visualize and diagnose diseases and conditions. However, manual segmentation of medical images is a time-consuming and error-prone task, requiring highly trained professionals. Automated segmentation of medical images can reduce the workload on clinicians while improving the accuracy and consistency of results. In this paper, the researchers present our solution to the HubMap Organ Segmentation Challenge, which aimed to accurately segment the glomeruli in human kidney tissue samples. The researchers used a combination of deep learning techniques and image processing to develop a sufficiently highly accurate segmentation model. The solution was based on a state-of-the-art convolutional neural network architecture, which was trained on a large dataset of labeled kidney tissue images. The researchers also conducted extensive experiments to evaluate the performance of our model on the test dataset provided by the competition. Our results demonstrated a high level of accuracy and outperformed the baseline models provided by the competition organizers.

1Research Student, Vellore Institute of Technology, Bhopal anubhavde2002@gmail.com
2Research Student, Vellore Institute of Technology, Bhopal vineet.joon2020@vitbhopal.ac.in
3Professor (SCSE), Vellore Institute of Technology, Bhopal nilamadhab.mishra@vitbhopal.ac.in

Major Highlights:

1. In this study, the researchers investigated the effects of different pre-trained models like EfficientNet, AlexNet, and ZFNet on the HubMAP - Organ Segmentation Dataset as part of the Kaggle Competition titled Hacking the Human Body.
2. The researchers then projected a customized model based on the U Net Architecture and CNN, and compared this model with the other pre-existing models to justify the claims.
3. The dataset consisting of data from two different consortia, the Human Protein Atlas (HPA) and Human BioMolecular Atlas Program (HuBMAP), was visualized and preprocessed.
4. The decreasing order of accuracy of the said models

was as follows: CNN+U Net > EfficientNet > ZFNet > AlexNet > CNN.

The rest of the paper is organized as follows; Section II addresses prior work and current approaches and techniques. The researchers then summarize the dataset and attribute distribution in Section III. Section IV delves into segmentation modeling, predicting the comparison of pre-trained models on the dataset, visualizing algorithms using neural networks, and visualizing the images from the dataset for better results. The evaluation metrics and experimental setup are all seen in Section V. It further demonstrates how the experiment was carried out and the findings obtained. Section VI provides code availability and Section VII concludes with a summary of existing work and several suggestions for potential improvements.

2. Related Work

Recently, machine learning (ML), a popular topic in image processing, has drawn a lot of interest from the medical community. The term "deep learning" (DL) for ANN refers specifically to ANN with multiple hidden layers and emerged from improvements in ANN structures and algorithms since 2006. The difference between ANN and DL is not precisely defined since there is disagreement about the number of layers that qualify as deep [1]. Multi-organ segmentation is the process of assigning each voxel of the medical images to one of the several labels that represent the objects of interest. Segmentation is one of the DL-based applications in the medical sector that is most often studied. As a result, there are numerous techniques and network topologies to choose from. The network architecture, training method (supervised, semi-supervised, unsupervised, transfer learning), input size (patch-based, full volume-based, 2D, 3D), and other attributes of DL-based multi-organ segmentation algorithms can be grouped into many categories. Researchers have tried to apply DL-based approaches to medical imaging to build on the success of DL in computer vision. In medical imaging, DL-based techniques have been thoroughly investigated for segmentation [2-9]. A significant advancement in radiation treatment procedures, DL-based multi-organ segmentation approaches speed up the segmentation process, improve contour uniformity, and encourage adherence to demarcation rules [2-3]. A simple way for automated segmentation that is accessible in many commercial solutions is the atlas-based method. This technique registers atlas templates with pre-contoured structures to the segmentation pictures, transmitting the pre-contoured structures to the new images. The precision of picture registration has a significant impact on the segmentation accuracy of this method. Accurate registration is not always ensured due to patient differences in organ morphology and picture artifacts. Using multi-atlas-based techniques with a vast and varied range of atlas datasets can help to solve this problem. However, it is challenging to incorporate all potential situations in the templates due to the unpredictable nature of tumor morphology. Deformable picture registration is also computationally expensive, and using a lot of atlas templates can drive up that cost significantly [10-12]. In medical images, anomalies, such as aberrant tissue types and atypical organ forms, are frequently present, making it difficult to derive ground truth labels for many organs for supervised learning. In automatic radiotherapy, organ segmentation in such an aberrant dataset is important. To identify organs in magnetic resonance imaging (MRI), Shin et al. used an SAE approach [13]. Numerous deep convolutional neural network models, including AlexNet [14], ZFNet [15], VGG [16], GoogleNet [17], Residual Net [18], DenseNet [19], FCN [20], and U-Net [21], have been suggested since 2012.In addition to providing a novel viewpoint on image fusion, these models provide state-of-the-art performance for image classification, segmentation, object recognition, and tracking tasks. The primary four factors influencing their success are as follows: First off, advances in neural networks are primarily responsible for deep learning's astounding success over conventional machine learning models. Deep learning learns high-level features incrementally from data, doing away with the requirement for hard feature extraction and domain knowledge. Additionally, it offers a comprehensive solution to the issue. Second, because of the advancement of GPUs and GPU-computing libraries, the model may be trained 10 to 30 times faster on GPUs than on CPUs. Additionally, effective GPU implementations are provided via open-source software packages. There are also some more reviews of deep learning-based medical picture analysis. They do not, however, concentrate on the fusion approach. For instance, Litjens et al.'s summary of the key deep learning ideas in medical image processing can be found at [22]. Using deep CNN, Bernal et al. [23] provided an overview of brain MRI analysis. In this study, the researchers concentrate on multi-modal medical image fusion techniques for medical picture segmentation.

3. Dataset Description

The dataset which the researchers have used for their work contains 706 files and has a size of around 9.39 GB of types such as TIFF, JSON, and CSV. This challenge's objective was to recognise each functional tissue unit (FTU) on biopsy slides taken from different organs. The underlying data consists of images from many sources that were created using various methods and resolutions, illustrating the common difficulties associated with working with medical data.

The Human Biomolecular Atlas Programme (HuBMAP) and the Human Protein Atlas (HPA), two separate consortia, provided the data for this competition. The training dataset is composed of public HPA data, the public test set is composed of private HPA data and HuBMAP data, and the private test set is composed solely of HuBMAP data. One of the main issues in this work will be getting models to work correctly when exposed to data that was produced using a different protocol.

1. **[train/test].csv** - Train/test set metadata. The test set's initial few rows are the only ones that can be downloaded.

- *Organ* - It is the organ from which the biopsy sample was collected,

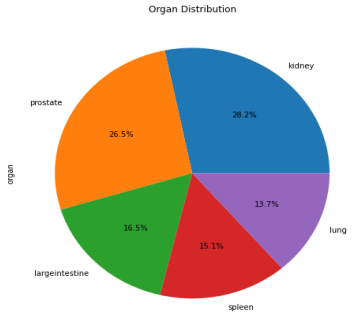

Fig 1: Organ Distribution

- *Id* - It is the picture ID.
- data source - It indicates whether HuBMAP or HPA provided the image.
- *img_height* - The image's height, expressed in pixels.
- *img_width* - The image's width, expressed in pixels.
- *pixel_size* - It is the height/width of a single pixel from this picture in micrometers. All HPA images have pixels that are 0.4 m in size. The kidney, large intestine, lung, spleen, and prostate all have pixel sizes of 0.5 m, 0.2290 m, 0.7562 m, and 6.263 m for HuBMAP pictures.

```
In [5]: display(train['data_source'].value_counts().to_frame())  # distribution of data source
        display(train['pixel_size'].value_counts().to_frame())  # distribution of pixel size
        display(train['tissue_thickness'].value_counts().to_frame())  # tissue thickness
```

data_source	
HPA	351

pixel_size	
0.4	351

tissue_thickness	
4	351

Fig.2: Displaying features - data_source, pixel_size, tissue_thickness

- *tissue_thickness* - The micrometer-measured thickness of the biopsy sample. The thickness of each HPA image is 4 m. The tissue slice thicknesses for the HuBMAP samples are 10 m for the kidney, 8 m for the large intestine, 4 m for the spleen, 5 m for the lung, and 5 m for the prostate
- *rle* - the desired column. a copy of the annotations with run-length encoding. only available during the training set.
- *patient's age* - It is expressed in years. only available during the training set.

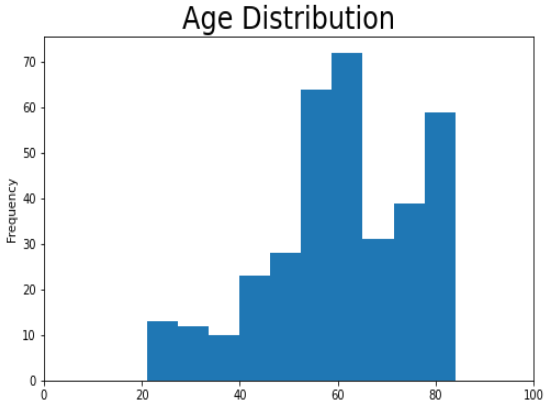

Fig 3: Age Distribution

- *sex* - The patient's sex. only available during the training set.

2. **sample_submission.csv** - It has two columns:

- rle - a run-length encoded mask of the image's FTUs.
- id - the image ID.

3. **[train/test]_images/** - The photos are in this. Expect the hidden test set to contain about 550 photos. Each HPA image has a tissue area that is approximately 2500 x 2500 pixels large and 3000 x 3000 pixels in size. The HuBMAP images have pixel sizes ranging from 4500x4500 to 160x160. Antibodies were used to stain HPA samples, which were then counterstained with hematoxylin and visualized using 3,3'-diaminobenzidine (DAB). Periodic acid-Schiff (PAS)/hematoxylin and eosin (H&E) stains were used to create HuBMAP pictures. There is at least one FTU in every image utilized. All tissue samples utilized in this competition came from

healthy donors whose tissue pathologists determined to be of low pathological interest.

4. **train_annotations/** - The annotations provided in the form of points that outline the limits of the FTUs' polygon masks are known as "train_annotations."

5. **HPA Data** - The HPA data consists of immunohistochemical images of tissue microarray cores that have been counterstained with hematoxylin (H)16,26 and visualized with 3,3'-diaminobenzidine (DAB) after being stained with antibodies. These cores have a diameter of 1 mm and a thickness of 4 m. The researchers obtained over 7TB of open data from the HPA, including 23,610 photographs of the large intestine and 27,906 images of 1 mm diameter tissue microarray (TMA) cores from the kidney, lung, and prostate. The HRA was created to capture human adults, thus the researchers removed any images of patients under the age of 18. After calculating sex, age, and tissue region percentages for each image, the 500 public photographs that maximize sex and age variety per organ, contain at least 1 FTU, and have a tissue region percentage above were selected. a threshold value (where the threshold value for the lung is 5% and the threshold values for the kidney, spleen, large intestine, and prostate are 15%).

The final dataset contains 432 open HPA pictures spread out among the five organs. The researchers also obtained from the HPA roughly 44GB of private (unpublished) data that included 253 large intestine photos, 295 kidney images, 291 lung images, 265 prostate images, and 290 spleen images. This dataset underwent the same processing as the publicly available HPA data. The final private dataset consisted of 81 photos in total. Except for 19 photographs that are between 2,308 by 2,308 and 3,070 by 3,070 pixels, all images, both public and private, are 3,000 px by 3,000 px in size.

5. **HuBMAP Data** - Multiple teams within or connected to HuBMAP contributed 257 unpublished periodic acid-Schiff (PAS)27 or hematoxylin and eosin (H&E)28 stain WSIs of healthy human tissue. 1mm tiles were extracted from these WSIs to match the size of the HPA TMA core images. The minimal donor information for all WSIs used in this competition was organ name, sex, and age. 448 image tiles total, distributed throughout the five organs, formed part of the final dataset, which came from five different teams. Except for the spleen, which allowed younger donors from 0 to 18, all organ donors were older than 18. The kidney had pixels that were 0.5 m in size, the large intestine was 0.229 m, the lung was 0.756 m, the spleen was 0.494 m, and the prostate was 6.263 m. Pictures in the HuBMAP data include tissue slice thicknesses ranging from 4 to 10 m, with the kidney, large intestine, spleen, lung, and prostate having a thickness of 10 m, 8 m, 4 m, and 5 m, respectively.

4. Data Preprocessing and Results

A. Discussion / Visualization –

The three winning teams in the "Hacking the Human Body" competition built model ensembles that included some or all vision transformer models, demonstrating the importance of these devices in biological image processing. This shows the rapid emergence of transformer models in the field and contrasts sharply with the last HuBMAP competition11 (which ended in May 2021), where all winning teams only employed convolutional models. It takes a lot of effort and money to find ground truth labels for supervised learning tasks, especially in the biomedical fields. The participants used a range of techniques, such as the inclusion of extra unlabeled data and the generation of pseudo-labels for training repeatedly to improve performance using a semi-supervised approach, to get around this problem. Together with skillful data augmentation and normalization techniques, this turned out to be the key.

Even though this competition offers several creative and effective solutions, these models have several drawbacks for actual production use cases:

1) Model overfitting is a possibility because the models were trained on a small dataset.
2) The vision transformer models are much more sensitive to data changes and hyperparameter tuning than the convolutional models, as teams discovered through numerous iterations of experiments.
3) Model ensembles are computationally expensive and might not be practical or efficient for many production settings.

By training and testing the models on more data in the future and condensing the enormous ensembles into a single model, the researchers hope to overcome the limitations outlined above. The HuBMAP data gateway will be used to handle massive volumes of tissue data and extract biological knowledge in support of the development and use of the winning models' software.

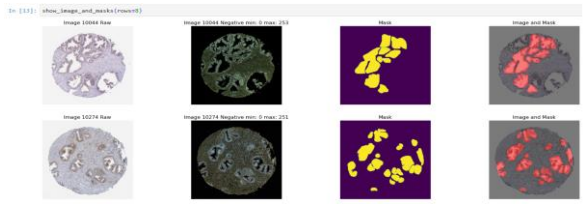

Fig. 4: Sample images of functional tissue units (FTU)

As depicted in the above Figure 4, the researchers have visualized the functional tissue unit images from the dataset in 4 ways: Raw Image, Negative Image, Mask & Image, and Masked images respectively. Only 2 rows from the dataset have been displayed here by the researchers, although the dataset may yield as many rows as there are images.

As depicted in Figure 5 given below, the researchers have created a function to display images from the training dataset which are masked from patches. The researchers have made use of visualization tools such as Numpy, and Matplotlib to build the function and its deployment. In the below sample images, the researchers have demonstrated and compared images of different organs in normal, masked, and combined forms for better visualization and study purpose.

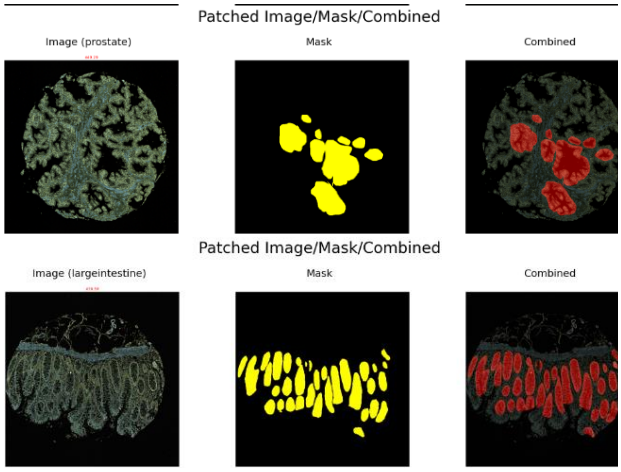

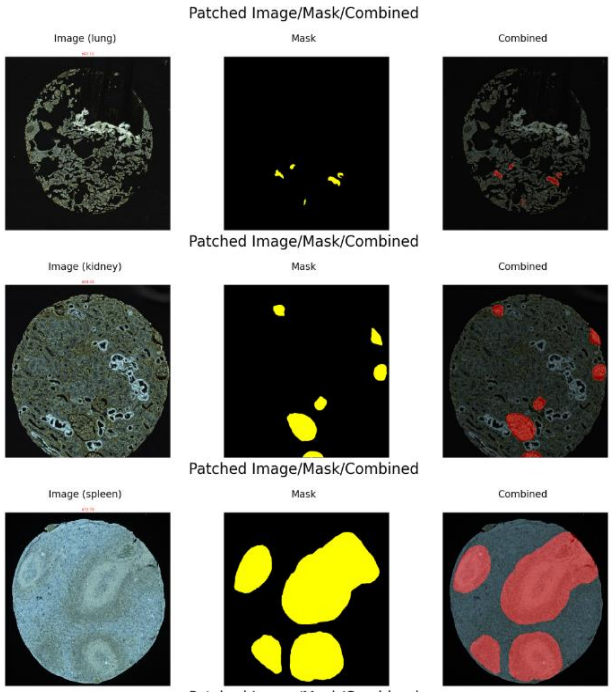

Fig.5: Samples of Patched Image vs Masked Image vs Combined Image of 5 different organs

Algorithms used –

The convolutional neural network known as *U-Net* was created for the segmentation of biological images. The network's architecture was expanded and changed from a fully convolutional network's original design to operate with fewer training photos and provide more accurate segmentation.

The *U-Net architecture* was used to train the final segmentation model to recognise the various tissue pictures. The positions of the various tissue pictures, such as the lung, spleen, large intestine, prostate, and kidney, were predicted using the trained segmentation model.

Fully Convolutional Networks used in previous versions of the model, are an architecture used mainly for semantic segmentation that gives us segmented images concerning the size of the image at the output.

C. ***Pre-Trained Models used*** **–**

1. *AlexNet*: AlexNet's convolutional neural network (CNN) has eight layers, including a classification-specific softmax layer, two fully connected layers, and five convolutional layers. AlexNet has shown to be effective for image segmentation tasks when used in conjunction with other techniques, such as fully convolutional networks (FCNs) or encoder-decoder architectures.
2. *ZFNet*: Five convolutional layers make up its structure, which is then followed by three fully

connected layers and a softmax layer at the end. The subsequent three convolutional layers have filters that are 3x3, whereas the first two have filters that are 7x7. The network also employs a max-pooling layer and a dropout layer. Originally designed for image classification tasks, it has been shown to perform well on several computer vision tasks, including object detection and segmentation.

3. *EfficientNet*: The foundation of EfficientNet models is a scaling technique that uses a predetermined set of preset scaling coefficients to scale the network's breadth, depth, and resolution equally. This allows for a balance between model size and accuracy, as the scaling coefficients control the tradeoff between these two factors. On a dataset of breast tissue images, prior research has demonstrated that an EfficientNet-based model outperformed a number of other well-known segmentation methods to attain state-of-the-art performance.

The tradeoff between model complexity and performance should be taken into account while comparing different models. In comparison to EfficientNet, AlexNet and ZFNet are noted for having deeper designs. This makes them more computationally expensive. EfficientNet is more resource- and memory-efficient because of its scaling approach, which enables it to attain competitive accuracy with a smaller model size.

The final decision on which model to use is determined by the details of the current picture classification task. AlexNet and ZFNet can both be good choices for situations where computing resources are not a major limitation, especially if fine-grained features are important. EfficientNet, on the other hand, offers a desirable option without compromising performance if resource utilization and efficiency are key considerations.

It is important to keep in mind that the performance comparison may change based on the dataset, job difficulty, and other elements. Therefore, it is advised to test and validate the model on the particular picture classification job before evaluating and choosing the best appropriate model.

5. Evaluations & Discussions

The mean Dice coefficient is used to judge the final submissions in CSV formats. A predicted segmentation's pixel-by-pixel agreement with the associated ground truth may be compared using the Dice coefficient. The formula is given by:

$$(2 * |A \cap B|) / (|A| + |B|)$$

here A represents the predicted set of pixels and B represents the actual ground truth. In the case where A & B are both empty, the Dice coefficient is 1. The average of the Dice coefficients for each picture in the test set is the leaderboard score.

Table 1: Comparative Performance Assessment

Models	Precision	Accuracy	F1 Score
CNN+ U Net	**0.852**	**0.84178**	**0.8392**
EfficientNet	0.807	0.80735	0.7986
ZFNet	0.783	0.77819	0.7643
AlexNet	0.772	0.76504	0.7529
CNN	0.711	0.71778	0.7088

As Table 1 presents, the researchers found out that U Net Architecture proved to be the most efficient on the dataset. Other pre-trained models such as EfficientNet, ZFNet, and AlexNet in respective order show significantly lesser accuracy on this dataset consisting of tissue images with an accuracy of 0.84178 using U Net and an accuracy of 0.71778 using a conventional Convolutional Neural Network.

The researchers conducted an extensive evaluation of different pre-trained models on the dataset of tissue images. The results indicated that the U-Net architecture exhibited the highest level of efficiency compared to other models, namely EfficientNet, ZFNet, and AlexNet.

Specifically, the U-Net architecture achieved an accuracy of 0.84178 on the dataset, outperforming the other models by a significant margin. This finding suggests that the U-Net architecture is particularly well-suited for the task of tissue image classification in the context of this study.

In contrast, when utilizing a conventional Convolutional Neural Network (CNN), the researchers observed a lower accuracy of 0.71778 on the same dataset. This further emphasizes the superior performance of the U-Net architecture in this specific domain.

The superior accuracy achieved by the U-Net architecture can have significant implications for applications in various fields. It demonstrates the effectiveness of U-Net in accurately classifying tissue images, which can be crucial in medical diagnostics, pathology, and other related areas. The ability to distinguish different tissue types with high accuracy can aid medical professionals in identifying abnormalities, making informed decisions, and providing better patient care.

However, it is important to note that the comparison of different models and their performance on the dataset is specific to this study. The findings may not be directly generalizable to other datasets or image classification tasks. Further research is necessary to validate and extend these findings to different contexts and datasets.

Overall, the evaluation results clearly indicate that the U-Net architecture outperformed other pre-trained models, including EfficientNet, ZFNet, and AlexNet, in terms of accuracy on the tissue image dataset. This finding underscores the potential of U-Net as a powerful tool for accurate tissue image classification and opens up opportunities for further exploration and development of this architecture in the field of medical image analysis.

6. Conclusion

The researchers offer a thorough analysis of recently released multi-organ segmentation techniques based on deep learning. The use of a fully convolutional network to conduct end-to-end multi-organ segmentation is clearly on the rise. This is so that end-to-end segmentation, which vastly speeds up segmentation, may benefit from the DL network's quick inference. Additionally becoming more common are methods for segmenting targets based on their areas before executing region-based Fully Convolutional Network (FCN) segmentation for each target.

The one-step multi-organ segmentation network may likewise provide strong segmentation results without needing to initially localize the target, therefore the region-based FCN has not yet seen widespread use. More datasets must be used to demonstrate the requirement of the initial organ localization phase in region-based FCN.

Another recent development is the use of synthetic images to enhance tissue contrast and boost segmentation realism. Synthetic image-aided segmentation's picture synthesis stage is not simple, however, which prevents widespread usage.

Beyond the lack of well-aligned paired pictures for synthesis network training, it is yet unknown how much value synthesis photos may provide to the segmentation job. Predicting appropriate organ borders in areas with limited picture contrast and few intensity gradients is a difficulty for segmentation. To regularize the segmentation findings, more organ shape restrictions are required.

Therefore, the researchers expect to see a steady growth of shape-constrained multi-organ segmentation. The results show the effectiveness of our approach and offer insights into organ segmentation in high-resolution histology images, which have significant applications in medical diagnosis and research. The results show that our approach achieves a score of 0.84178 using U Net Architecture which was calculated with approximately 45% of the test data thereby securing a rank in the top 28% among 1175 participants across the globe.

7. Data Availability

The public may access all of the competition's data, training models, preprocessing and analysis code, and trained models on GitHub at *https://github.com/n1ghtf4l1/automatic-dissection*.

8. References and Footnotes

Acknowledgements

We thank our colleagues from Vellore Institute of Technology, Bhopal who provided insight and expertise that greatly assisted the research, although they may not agree with all of the interpretations/conclusions of this paper. We thank Nilamadhab Mishra, Associate Professor [SCSE] Vellore Institute of Technology, Bhopal for assistance with reviewing, editing and comments that greatly improved the manuscript.

Author contributions

Anubhav De: Data curation, Conceptualization, Validation, Methodology, Software, Field study **Vineet Joon:** Data curation, Writing-Original draft preparation, Software, Validation., Field study **Nilamadhab Mishra:** Investigation, Writing-Reviewing and Editing.

Conflicts of interest

The authors declare no conflicts of interest.

References

[1] Yang Lei, Tonghe Wang, Joseph Harms, Yabo Fu, Xue Dong, Walter J. Curran, Tian Liu, and Xiaofeng Yang. Cbct-based synthetic mri generation for cbct-guided adaptive radiotherapy. In Dan Nguyen, Lei Xing, and Steve Jiang, editors, Artificial Intelligence in Radiation Therapy, pages 154–161. Springer International Publishing, . ISBN 978-3-030-32486-5.

[2] X. Dong, Y. Lei, S. Tian, T. Wang, P. Patel, W. J. Curran, A. B. Jani, T. Liu, and X. Yang. Synthetic mri-aided multi-organ segmentation on male pelvic ct using cycle consistent deep attention network. Radiother Oncol, 141:192–199, 2019. ISSN 0167-8140. doi: 10.1016/j.radonc.2019.09.028.

[3] X. Dong, Y. Lei, T. Wang, M. Thomas, L. Tang, W. J. Curran, T. Liu, and X. Yang. Automatic multiorgan segmentation in thorax ct images using u-net-gan. Med Phys, 46(5):2157–2168, 2019. ISSN 0094-2405. doi: 10.1002/mp.13458.

[4] Y. Lei, X. Dong, Z. Tian, Y. Liu, S. Tian, T. Wang, X. Jiang, P. Patel, A. B. Jani, H. Mao, W. J. Curran, T. Liu, and X. Yang. Ct prostate segmentation based on synthetic mri-aided deep attention fully convolution network. Med Phys, 2019. ISSN 0094-2405. doi: 10.1002/mp.13933.

[5] Y. Lei, X. Dong, T. Wang, K. Higgins, T. Liu, W. J. Curran, H. Mao, J. A. Nye, and X. Yang. Wholebody pet estimation from low count statistics using cycle-consistent generative adversarial networks. Phys Med Biol, 64(21):215017, 2019. ISSN 0031-9155. doi: 10.1088/1361-6560/ab4891.

[6] Y. Lei, S. Tian, X. He, T. Wang, B. Wang, P. Patel, A. B. Jani, H. Mao, W. J. Curran, T. Liu, and X. Yang. Ultrasound prostate segmentation based on multidirectional deeply supervised v-net. Med Phys, 46(7):3194–3206, 2019. ISSN 0094-2405. doi: 10.1002/mp.13577.

[7] Y. Lei, T. Wang, S. Tian, X. Dong, A. B. Jani, D. Schuster, W. J. Curran, P. Patel, T. Liu, and X. Yang. Male pelvic multi-organ segmentation aided by cbct-based synthetic mri. Phys Med Biol, 2019. ISSN 0031-9155. doi: 10.1088/1361-6560/ab63bb.

[8] Bo Wang, Yang Lei, Jiwoong Jason Jeong, Tonghe Wang, Yingzi Liu, Sibo Tian, Pretesh Patel, Xiaojun Jiang, Ashesh B. Jani, Hui Mao, Walter J. Curran, Tian Liu, and Xiaofeng Yang. Automatic MRI prostate segmentation using 3D deeply supervised FCN with concatenated atrous convolution. In Kensaku Mori and Horst K. Hahn, editors, Medical Imaging 2019: Computer-Aided Diagnosis, volume 10950, pages 988 – 995. International Society for Optics and Photonics, SPIE, 2019. doi: 10.1117/12.2512551. URL https://doi.org/10.1117/12.2512551.

[9] Bo Wang, Yang Lei, Tonghe Wang, Xue Dong, Sibo Tian, Xiaojun Jiang, Ashesh B. Jani, Tian Liu, Walter J. Curran, Pretesh Patel, and Xiaofeng Yang. Automated prostate segmentation of volumetric CT images using 3D deeply supervised dilated FCN. In Elsa D. Angelini and Bennett A. Landman, editors, Medical Imaging 2019: Image Processing, volume 10949, pages 708 – 715. International Society for Optics and Photonics, SPIE, 2019. doi: 10.1117/12.2512547. URL https://doi.org/10.1117/12.2512547.

[10] S. H. Sun, C. Bauer, and R. Beichel. Automated 3-d segmentation of lungs with lung cancer in ct data using a novel robust active shape model approach. Ieee Transactions on Medical Imaging, 31 (2):449–460, 2012. ISSN 0278-0062. doi: 10.1109/Tmi.2011.2171357. URL ://WOS: 000300197500025.

[11] A. A. Qazi, V. Pekar, J. Kim, J. Xie, S. L. Breen, and D. A. Jaffray. Auto-segmentation of normal and target structures in head and neck ct images: A feature-driven model-based approach. Medical Physics, 38(11):6160–6170, 2011. ISSN 0094-2405. doi: 10.1118/1.3654160. URL : //WOS:000296534000037.

[12] Xue Feng, Kun Qing, Nicholas J. Tustison, Craig H. Meyer, and Quan Chen. Deep convolutional neural network for segmentation of thoracic organs-at-risk using cropped 3d images. Medical Physics, 46(5):2169–2180, 2019. ISSN 0094-2405. doi: 10.1002/mp.13466. URL https://doi. org/10.1002/mp.13466.

[13] H. C. Shin, M. R. Orton, D. J. Collins, S. J. Doran, and M. O. Leach. Stacked autoencoders for unsupervised feature learning and multiple organ detection in a pilot study using 4d patient data. Ieee Transactions on Pattern Analysis and Machine Intelligence, 35(8):1930–1943, 2013. ISSN 0162-8828. doi: 10.1109/Tpami.2012.277. URL ://WOS:000320381400009.

[14] Krizhevsky A, Sutskever I, Hinton GE. Imagenet classification with deep convolutional neural networks. In: Advances in neural information processing systems. Advances in neural information processing systems; 2012. p. 1097–105.

[15] Zeiler MD, Fergus R. Visualizing and understanding convolutional networks. In: European

conference on computer vision. Springer; 2014. p. 818–33.
[16] K. Simonyan, A. Zisserman, Very deep convolutional networks for largescale image recognition, arXiv preprint arXiv:1409.1556
[17] Szegedy C, Liu W, Jia Y, Sermanet P, Reed S, Anguelov D, Erhan D, Vanhoucke V, Rabinovich A. Going deeper with convolutions. In: Proceedings of the IEEE conference on computer vision and pattern recognition; 2015. p. 1–9.
[18] He K, Zhang X, Ren S, Sun J. Identity mappings in deep residual networks. In: European conference on computer vision. Springer; 2016. p. 630–45.
[19] Huang G, Liu Z, Van Der Maaten L, Weinberger KQ. Densely connected convolutional networks. In: Proceedings of the IEEE conference on computer vision and pattern recognition; 2017. p. 4700–8.
[20] Long J, Shelhamer E, Darrell T. Fully convolutional networks for semantic segmentation. In: Proceedings of the IEEE conference on computer vision and pattern recognition; 2015. p. 3431–40.
[21] Ronneberger O, Fischer P, Brox T, U-net. Convolutional networks for biomedical image segmentation. In: International Conference on Medicalimage computing and computer-assisted intervention. Springer; 2015. p. 234–41.
[22] Litjens G, Kooi T, Bejnordi BE, Setio AAA, Ciompi F, Ghafoorian M, Van Der Laak JA, Van Ginneken B, S_anchez CI. A survey on deep learning in medical image analysis. Med Image Anal 2017;42:60–88.
[23] J. Bernal, K. Kushibar, D. S. Asfaw, S. Valverde, A. Oliver, R. Martí, X. Lladoo, Deep convolutional neural networks for brain image analysis on magnetic resonance imaging: a review, Artif. Intell. Med..
[24] Guoheng Huang, Junwen Zhu, Jiajian Li, Zhuowei Wang, Lianglun Cheng, Lizhi Liu, Haojiang Li, Jian Zhou. "Channel-Attention U-Net: Channel Attention Mechanism for Semantic Segmentation of Esophagus and Esophageal Cancer", IEEE Access, 2020
[25] Haodong Chen, Niloofar Zendehdel, Ming C. Leu, Zhaozheng Yin. "Multi-Modal Fine-Grained Activity Recognition and Prediction in Assembly", Research Square Platform LLC, 2022
[26] "Engineering Applications of Neural Networks", Springer Science and Business Media LLC, 2017
[27] "Scientific Abstracts and Sessions", Medical Physics, 2018
[28] "Deep Learning for Cancer Diagnosis", Springer Science and Business Media LLC, 2021
[29] Keerthana B. Chigateri, Ajit M. Hebbale. "A steel surface defect detection model using machine learning", Materials Today: Proceedings, 2023
[30] Yashvardhan Jain, Leah L. Godwin, Sripad Joshi, Shriya Mandarapu, Trang Le, Cecilia Lindskog, Emma Lundberg, Katy Börner. "Segmenting functional tissue units across human organs using community-driven development of generalizable machine learning algorithms", Cold Spring Harbor Laboratory, 2023
[31] Yabo Fu, Yang Lei, Tonghe Wang, Walter J. Curran, Tian Liu, Xiaofeng Yang. "A review of deep learning based methods for medical image multi-organ segmentation", Physica Medica, 2021
[32] "Scientific Abstracts and Sessions", Medical Physics, 2020
[33] Chandraprabha, M. ., & Dhanaraj, R. K. . (2023). Adaboost CNN with Horse Herd Optimization Algorithm to Forecast the Rice Crop Yield . International Journal on Recent and Innovation Trends in Computing and Communication, 11(4), 192–203. https://doi.org/10.17762/ijritcc.v11i4.6401
[34] Auma, G., Levi, S., Santos, M., Ji-hoon, P., & Tanaka, A. Predicting Stock Market Trends using Long Short-Term Memory Networks. Kuwait Journal of Machine Learning, 1(3). Retrieved from http://kuwaitjournals.com/index.php/kjml/article/view/136
[35] Pandey, J. K., Veeraiah, V., Talukdar, S. B., Talukdar, V., Rathod, V. M., & Dhabliya, D. (2023). Smart city approaches using machine learning and the IoT. Handbook of research on data-driven mathematical modeling in smart cities (pp. 345-362) doi:10.4018/978-1-6684-6408- 3.ch018 Retrieved from www.scopus.com